

CONJUGATED HEAT TRANSFER IN MICROCHANNELS

J.S. NUNES^{1 A,B}, R.M. COTTA^A, M.R. AVELINO^C,
S. KAKAÇ^D

^A Laboratory of Transmission and Technology of Heat, LTTC
Mechanical Engineering Dept., COPPE & POLI - C.P. 68503
CEP 21945-970 - Universidade Federal do Rio de Janeiro, RJ
Brasil

^B INPI, Rio de Janeiro, RJ, Brasil

^C Universidade do Estado do Rio de Janeiro, UERJ, Rio de
Janeiro, Brasil

^D TOBB University of Economics & Technology, Ankara,
Turkey

1. Introduction

Energy conservation and sustainable development demands have been driving research efforts, within the scope of thermal engineering, towards more energy efficient equipments and processes. In this context, the scale reduction in mechanical fabrication has been permitting the miniaturization of thermal devices, such as in the case of micro-heat exchangers [1]. More recently, heat exchangers employing micro-channels with characteristic dimensions below 500 microns have been calling the attention of researchers and practitioners, towards applications that require high heat removal demands and/or space and weight limitations [2]. Recent review works [2,3] have pointed out discrepancies between experimental results and classical correlation predictions of heat transfer coefficients in micro-channels. Such deviations have been stimulating theoretical research efforts towards a better agreement between experiments and simulations, through the incorporation of different effects that are either typically present in micro-scale heat transfer or are effects that are normally disregarded at the macro-scale and might have been erroneously not accounted for in micro-channels. Our own research effort was first related to the fundamental analysis of forced convection within micro-channels with and without slip flow, as required for the design of micro-heat exchangers in steady, periodic and transient regimen [4-5]. Also recently in [6-11], the analytical contributions were directed towards more general problem formulations,

including viscous dissipation, axial diffusion in the fluid and three-dimensional flow geometries. Then, this fundamental research was extended to include the effects of axial fluid heat conduction and wall corrugation on heat transfer enhancement [12]. The work of Maranzana et al. [13] further motivated the present analysis, dealing with longitudinal wall heat conduction effects in symmetric micro-channels.

Conjugated conduction-convection problems are among the classical formulations in heat transfer that still demand exact analytical treatment. Since the pioneering works of Perelman (1961) [14] and Luikov et al. (1971) [15], such class of problems continuously deserved the attention of various researchers towards the development of approximate formulations and/or solutions, either in external or internal flow situations. For instance, the here employed integral transform approach itself has been applied to obtain hybrid solutions for conjugated conduction-convection problems [16-21], in both steady and transient formulations, by employing a transversally lumped or improved lumped heat conduction equation for the wall temperature.

The present work then illustrates theoretical-experimental research efforts on forced convection in micro-channels, trying to focus on the fundamental aspects that are required to play some role in matching the classical heat transfer models to available or produced experimental results in laminar forced convection. The first aim was to address the walls conjugation effects for a parallel-plates micro-channel, micro-machined from metallic plates, subjected to asymmetric thermal boundary conditions. The typical low Reynolds numbers in such micro-systems may lead to low values of the Peclet number that bring up some relevance to the axial heat diffusion along the fluid stream, especially for regions close to the inlet. Thus, both the bounding walls and the fluid axial diffusion may participate in the overall heat transfer process, and yield different predictions than those reached by making use of conventional macro-scale relations for ordinary liquids.

All the theoretical work was performed by making use of mixed symbolic-numerical computation via the *Mathematica 7.0* platform [22], and a hybrid numerical-analytical methodology with automatic error control, the Generalized Integral Transform Technique – GITT [23-26], in handling the governing partial differential equations.

An experimental setup was designed and built for the determination of Nusselt numbers in a parallel plates channel made of brass and copper inside a PMMA (poly-methyl methacrylate) prism, with Joule effect heating on the brass side. Experimental runs for different Reynolds numbers allowed for obtaining a significant set of experimental results for a micro-channel height of 270 microns. Experimental results are then briefly discussed and presented to verify the proposed model.

2. Theoretical Analysis

The objective of this research was to theoretically and experimentally analyze the conjugated heat transfer problem in micro-scale for laminar flow, involving the simultaneous determination of the temperature fields in the liquid and solid regions of a rectangular micro-channel formed by parallel plates made of distinct materials and subjected to asymmetric thermal conditions. The methodology that has been applied in the modeling and solution of this problem consists in the application of the Lumped System Approach to the solid boundaries adjacent to fluid, which are then transformed into boundary conditions for the convection problem and, subsequently, applying the Generalized Integral Transform Technique (GITT) [23-26] to obtain an ordinary differential formulation for the transformed fluid temperatures, solved by an adequate routine in the *Mathematica* computational platform [22]. An experimental setup was designed and built for the determination of Nusselt numbers in a parallel plate channel made of brass and copper, with Joule effect heating on one side and adjustable distance between the plates, offering comparisons and validation of the proposed model.

We thus consider thermally developing forced convection of a Newtonian fluid in the continuum regimen, under fully developed laminar flow inside a rectangular micro-channel formed by parallel layers of different materials and/or thicknesses, and subjected to an inlet temperature T_e . The walls are assumed to participate in the heat transfer process within the fluid along the channel length, and to exchange heat with the external environment with the temperature T_{ext} and a heat transfer coefficient h_{ext} , according to Figure 1 below. In addition, the walls are allowed to uniformly generate heat.

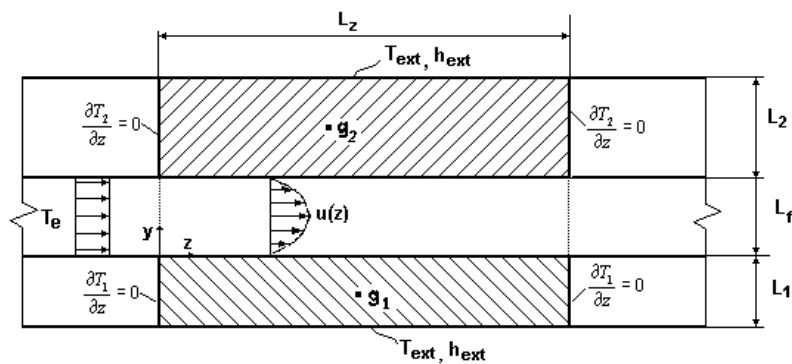


Figure 1. Geometry and coordinates system for asymmetric conjugated heat transfer in micro-channels.

4 CONJUGATED HEAT TRANSFER IN MICROCHANNELS

The thermophysical properties of all the materials are taken as constant and the conjugated problem can be written in dimensionless form as follows:

$$\frac{\partial^2 \theta_1}{\partial \eta^2} + \frac{1}{(2Pe)^2} \frac{\partial^2 \theta_1}{\partial \zeta^2} + Q_1 = 0; \quad -l_{\eta_1} < \eta < 0; \quad 0 < \zeta < l_\zeta \quad (1a)$$

$$\frac{U(\eta)}{4} \frac{\partial \theta_f}{\partial \zeta} = \frac{\partial^2 \theta_f}{\partial \eta^2} + \frac{1}{(2Pe)^2} \frac{\partial^2 \theta_f}{\partial \zeta^2} + Br \left(\frac{dU(\eta)}{d\eta} \right)^2 \quad 0 < \eta < 1 \quad \zeta > 0 \quad (1b)$$

$$\frac{\partial^2 \theta_2}{\partial \eta^2} + \frac{1}{(2Pe)^2} \frac{\partial^2 \theta_2}{\partial \zeta^2} + Q_2 = 0; \quad 1 < \eta < l_{\eta_2} \quad 0 < \zeta < l_\zeta \quad (1c)$$

where the three energy equations above refer, respectively, to the lower wall, to the fluid and to the upper wall in Figure 1. The following boundary and inlet conditions are proposed:

$$\frac{\partial \theta_1}{\partial \zeta} = 0 \quad \zeta = 0, \quad \frac{\partial \theta_1}{\partial \zeta} = 0 \quad \zeta = l_\zeta \quad (2a,b)$$

$$\frac{\partial \theta_2}{\partial \zeta} = 0 \quad \zeta = 0, \quad \frac{\partial \theta_2}{\partial \zeta} = 0 \quad \zeta = l_\zeta \quad (2c,d)$$

$$-\frac{\partial \theta_1}{\partial \eta} + Bi_{\eta_1} \theta_1 = 0 \quad \eta = -l_{\eta_1}, \quad \frac{\partial \theta_2}{\partial \eta} + Bi_{\eta_2} \theta_2 = 0 \quad \eta = l_{\eta_2} \quad (2e,f)$$

$$\theta_f(\eta, \zeta) = 1 \quad \zeta = 0, \quad \frac{\partial \theta_f}{\partial \zeta} = 0 \quad \zeta = l_\zeta \quad (2g,h)$$

besides the interface conditions

$$\theta_f = \theta_1 \quad \eta = 0, \quad k_1^* \frac{\partial \theta_f}{\partial \eta} = \frac{\partial \theta_1}{\partial \eta} \quad \eta = 0 \quad (2i,j)$$

$$\theta_f = \theta_2 \quad \eta = 1 \quad 0 < \zeta < l_\zeta, \quad k_2^* \frac{\partial \theta_f}{\partial \eta} = \frac{\partial \theta_2}{\partial \eta} \quad \eta = 1 \quad 0 < \zeta < l_\zeta \quad (2k,l)$$

The following dimensionless relations were here employed:

$$\theta_i = \frac{T_i - T_\infty}{T_0 - T_\infty}, \text{ where } i = 1, 2, f; \quad \zeta = \frac{z}{\text{Pr Re } D_h}; \quad \eta = \frac{y}{L_f};$$

$$D_h = \frac{4S}{P} \Rightarrow \frac{4(L_f^* L_w)}{2(L_f + L_w)}, \text{ since } L_w \gg L_f \Rightarrow D_h = 2L_f; \quad (3a-k)$$

$$U(\eta) = \frac{u(y)}{\bar{u}}; \quad \frac{d\zeta}{dz} = \frac{1}{\text{Pr Re } Dh}; \quad \frac{d\eta}{dy} = \frac{1}{L_f};$$

$$\text{Pe} = \text{Re Pr}; \quad \text{Re} = \frac{\bar{u} D_h}{\nu}; \quad u(y) = 3y(1-2y)$$

and,

$$Q_1 = \frac{g_1 L_f^2}{k_1 \Delta T}, \quad W(\eta) = \frac{U(\eta)}{4}, \quad Q_2 = \frac{g_2 L_f^2}{k_2 \Delta T} \quad \text{and} \quad \text{Br} = \frac{\mu u}{k \Delta T} \quad (3l-o)$$

$$k_1^* = \frac{k_f}{k_1}; \quad k_2^* = \frac{k_f}{k_2}; \quad l_{\eta 1} = \frac{L_1}{L_f}, \quad l_{\eta 2} = \frac{L_2 + L_f}{L_f} \quad (3p-s)$$

where the indexes 1 and 2 denote the lower and upper solid layers, and f refers to the fluid.

The Classic Lumped System Analysis is applied to the energy equations of the two solid layers that define the walls of the channel. This reformulation and simplification strategy is feasible once the temperature gradients across both walls are sufficiently smooth, a behavior governed by the magnitudes of the Biot numbers at each face of the two walls. For instance, considering the thermally thin-walled hypothesis for layer 1 above, the lumping procedure assumes that

$$\theta_1(-l_{\eta 1}, \zeta) \cong \theta_1(0, \zeta) \cong \theta_{av,1}(\zeta) \quad (4a)$$

where $\theta_{av,1}(\zeta)$ is calculated by the transversally averaged temperature definition:

$$\theta_{av,1}(\zeta) = \frac{1}{l_{\eta 1}} \int_{-l_{\eta 1}}^0 \theta_1(\eta, \zeta) d\eta \quad (4b)$$

Equation (1a) for $\theta_1(\eta, \zeta)$ is thus integrated in the η direction, applying the integral operator $\frac{1}{l_{\eta 1}} \int_{-l_{\eta 1}}^0 \dots d\eta$ in both the energy equation and required boundary conditions, providing after some manipulation:

$$-\frac{\partial \theta_f}{\partial \eta} + \text{Bi}_{\eta 1}^* \theta_f = \frac{l_{\eta 1}}{(2\text{Pe})^2} \frac{\partial^2 \theta_f(\eta, \zeta)}{\partial \zeta^2} \Big|_{\eta=0} + Q_1^* \quad \eta = 0 \quad (5a)$$

where

$$Bi_{\eta_1}^* = \frac{Bi_{\eta_1}}{k_1^*} \quad \text{and} \quad Q_1^* = \frac{l_{\eta_1}}{k_1^*} Q_1 \quad (5b,c)$$

The same procedure is then applied to layer 2, Eq.(1c), which results in:

$$\frac{\partial \theta_f}{\partial \eta} + Bi_{\eta_2}^* \theta_f = \frac{(l_{\eta_2} - 1)}{k_2^* (2Pe)^2} \frac{\partial^2 \theta_f(\eta, \zeta)}{\partial \zeta^2} \Big|_{\eta=1} + Q_2^* \quad \eta = 1 \quad (5d)$$

where

$$Bi_{\eta_2}^* = \frac{Bi_{\eta_2}}{k_2^*} \quad \text{and} \quad Q_2^* = \frac{(l_{\eta_2} - 1)}{k_2^*} Q_2 \quad (5e,f)$$

Thus, application of the lumping procedure to the original formulation leads to the extended Graetz problem described by the equation and boundary conditions below:

$$W(\eta) \frac{\partial \theta_f}{\partial \zeta} = \frac{\partial^2 \theta_f}{\partial \eta^2} + \frac{1}{(2Pe)^2} \frac{\partial^2 \theta_f}{\partial \zeta^2} + Br \left(\frac{dU(\eta)}{d\eta} \right)^2, \quad 0 < \eta < 1, \quad \zeta > 0 \quad (6a)$$

$$-\frac{\partial \theta_f}{\partial \eta} + Bi_{\eta_1}^* \theta_f = Cj_1 \frac{\partial^2 \theta_f(\eta, \zeta)}{\partial \zeta^2} + Q_1^*, \quad \eta = 0 \quad (6b)$$

$$\frac{\partial \theta_f}{\partial \eta} + Bi_{\eta_2}^* \theta_f = Cj_2 \frac{\partial^2 \theta_f(\eta, \zeta)}{\partial \zeta^2} + Q_2^*, \quad \eta = 1 \quad (6c)$$

$$\theta_f(\eta, \zeta) = 1 \quad \zeta = 0, \quad \frac{\partial \theta_f}{\partial \eta} = 0 \quad \zeta = l_\zeta \quad (6d,e)$$

where Cj_1 and Cj_2 are the conjugation coefficients, respectively, in the lower and upper walls, as:

$$Cj_1 = \frac{l_{\eta_1}}{(2Pe)^2 k_1^*}; \quad Cj_2 = \frac{l_{\eta_2} - 1}{(2Pe)^2 k_2^*} \quad (6f,g)$$

Eqs. (6) are now solved by the Generalized Integral Transform Technique, GITT, starting with the choice of an appropriate filtering solution that eliminates the non-homogeneous terms in the equation and boundary conditions:

$$\theta_f(\eta, \zeta) = \theta_H(\eta, \zeta) + \theta_p(\eta) \quad (7)$$

A fairly simple filter in terms of a purely diffusive formulation in the transversal direction is proposed:

$$\frac{d^2\theta_p(\eta)}{d\eta^2} + Br \left(\frac{d(U(\eta))}{d\eta} \right)^2 = 0 \quad 0 < \eta < 1 \quad \zeta > 0 \quad (8a)$$

$$\begin{aligned} -\frac{d\theta_p(\eta)}{d\eta} + Bi_{\eta_1}^* \theta_p(\eta) &= Q_1^* & \eta = 0 \\ \frac{d\theta_p(\eta)}{d\eta} + Bi_{\eta_2}^* \theta_p(\eta) &= Q_2^* & \eta = 1 \end{aligned} \quad (8b,c)$$

The filtered problem formulation is then given by:

$$W(\eta) \frac{\partial \theta_H(\eta, \zeta)}{\partial \zeta} - \frac{1}{(2Pe)^2} \frac{\partial^2 \theta_H(\eta, \zeta)}{\partial \zeta^2} = \frac{\partial^2 \theta_H(\eta, \zeta)}{\partial \eta^2} \quad 0 < \eta < 1 \quad \zeta > 0 \quad (9a)$$

$$\theta_H(\eta, \zeta) = 1 - \theta_p(\eta), \quad \zeta = 0; \quad \frac{\partial \theta_H(\eta, \zeta)}{\partial \eta} = 0, \quad \zeta = l_\zeta \quad (9b,c)$$

$$\begin{aligned} -\frac{\partial \theta_H(\eta, \zeta)}{\partial \eta} + Bi_{\eta_1}^* \theta_H(\eta, \zeta) &= Cj_1 \frac{\partial^2 \theta_H(\eta, \zeta)}{\partial \zeta^2} & \eta = 0 \\ \frac{\partial \theta_H(\eta, \zeta)}{\partial \eta} + Bi_{\eta_2}^* \theta_H(\eta, \zeta) &= Cj_2 \frac{\partial^2 \theta_H(\eta, \zeta)}{\partial \zeta^2} & \eta = 1 \end{aligned} \quad (9d,e)$$

The auxiliary problem that forms the basis for the eigenfunction expansion is then proposed:

$$\frac{d^2\psi_i(\eta)}{d\eta^2} + \beta_i^2 W(\eta) \psi_i(\eta) = 0, \quad 0 < \eta < 1 \quad (10a)$$

$$-\frac{d\psi_i(\eta)}{d\eta} + Bi_{\eta_1}^* \psi_i(\eta) = 0, \quad \eta = 0; \quad \frac{d\psi_i(\eta)}{d\eta} + Bi_{\eta_2}^* \psi_i(\eta) = 0, \quad \eta = 1 \quad (10b,c)$$

Then, the integral transform pair is constructed for application of the GITT:

$$\begin{cases} \bar{\theta}_i(\zeta) = \int_0^1 W(\eta) \psi_i(\eta) \theta_H(\eta, \zeta) d\eta & \text{transform} \\ \theta_H(\eta, \zeta) = \sum_{i=1}^{\infty} \frac{\psi_i(\eta)}{N_i} \bar{\theta}_i(\zeta) & \text{inverse} \end{cases} \quad (11a,b)$$

where the norm is given by:

$$N_i = \int_0^1 W(\eta) \psi_i(\eta)^2 d\eta \quad (11c)$$

Using the integral operator in Eq. (11a) and applying the 2nd Green's formula, the transformed system is given by:

$$\frac{d\bar{\theta}_i(\zeta)}{d\zeta} + \beta_i^2 \bar{\theta}_i(\zeta) = C_{j_1} \psi_i(0) \frac{\partial^2 \theta_H}{\partial \zeta^2} \Big|_{\eta=0} + C_{j_2} \psi_i(1) \frac{\partial^2 \theta_H}{\partial \zeta^2} \Big|_{\eta=1} + \frac{1}{(2Pe)^2} \int_0^1 \psi_i(\eta) \frac{\partial^2 \theta_H}{\partial \zeta^2} d\eta \quad (12a)$$

Employing the inverse formula in the axial diffusion term, $\frac{1}{(2Pe)^2} \int_0^1 \psi_i(\eta) \frac{\partial^2 \theta_H}{\partial \zeta^2} d\eta$, we find:

$$\sum_{j=1}^{\infty} \frac{1}{(2Pe)^2} \frac{d^2 \bar{\theta}_j(\zeta)}{d\zeta^2} \frac{1}{N_j} \underbrace{\int_0^1 \psi_i(\eta) \psi_j(\eta) d\eta}_{I\psi_{ij}} = \sum_{j=1}^{\infty} \frac{1}{(2Pe)^2} \frac{d^2 \bar{\theta}_j(\zeta)}{d\zeta^2} \frac{I\psi_{ij}}{N_j} \quad (12b)$$

Replacing directly into Eq.(12a) the relations found in the modified boundary conditions, Eqs. (9d,e), we have:

$$\begin{aligned} \frac{d\bar{\theta}_i(\zeta)}{d\zeta} + \beta_i^2 \bar{\theta}_i(\zeta) = & \psi_i(0) \left(-\frac{\partial \theta_H}{\partial \eta} \Big|_{\eta=0} + Bi_{\eta_1}^* \theta_{w_1}(\zeta) \right) + \psi_i(1) \left(\frac{\partial \theta_H}{\partial \eta} \Big|_{\eta=1} + Bi_{\eta_2}^* \theta_{w_2}(\zeta) \right) + \\ & + \sum_{j=1}^{\infty} \frac{1}{(2Pe)^2} \frac{d^2 \bar{\theta}_j(\zeta)}{d\zeta^2} \frac{I\psi_{ij}}{N_j} \quad 0 < \eta < 1 \quad \zeta > 0 \end{aligned} \quad (12c)$$

where $\theta_{w_1}(\zeta) = \theta_f(0, \zeta)$ and $\theta_{w_2}(\zeta) = \theta_f(1, \zeta)$.

After substitution of the inverse formulae in the remaining terms, and some rearrangement, the transformed ODE system is written as:

$$\begin{aligned} \sum_{j=1}^{\infty} aa_{ij} \frac{d^2 \bar{\theta}_j(\zeta)}{d\zeta^2} - \sum_{j=1}^{\infty} \delta_{ij} \frac{d\bar{\theta}_j(\zeta)}{d\zeta} - \sum_{j=1}^{\infty} a_{ij} \bar{\theta}_j(\zeta) = \\ - [g_{1i} \theta_{w_1}(\zeta) + g_{2i} \theta_{w_2}(\zeta)]_i \quad 0 < \eta < 1 \quad \zeta > 0 \end{aligned} \quad (13a)$$

where

$$\mathbf{A} = \{a_{ij}\} \begin{cases} \beta_i^2 - \frac{1}{N_j} \left(\psi_i(1) \frac{d\psi_i}{d\eta} \Big|_{\eta=1} - \psi_i(0) \frac{d\psi_i}{d\eta} \Big|_{\eta=0} \right) & i \leq N \quad j \leq N \quad i = j \\ -\frac{1}{N_j} \left(\psi_i(1) \frac{d\psi_j}{d\eta} \Big|_{\eta=1} - \psi_i(0) \frac{d\psi_j}{d\eta} \Big|_{\eta=0} \right) & i \leq N \quad j \leq N \quad i \neq j \end{cases} \quad (13b,c)$$

$$[AA] = \{aa_{ij}\} = \frac{1}{(2Pe)^2} \frac{I\psi_{ij}}{N_j} \quad \forall i, j \begin{cases} i \leq N \\ j \leq N \end{cases} \quad (13d)$$

$$g_1 = \{Bi_{\eta_1}^* \psi_i(0)\}, \quad g_2 = \{Bi_{\eta_2}^* \psi_i(1)\}, \quad i \leq N \quad (13e,f)$$

The equations that govern the wall temperatures are then rewritten as:

$$\begin{aligned}\frac{d\theta_{w1}'}{d\zeta} &= -\frac{1}{Cj_1} \sum_{j=1}^N \frac{1}{N_j} \frac{\partial \psi_j}{\partial \eta} \Big|_{\eta=0} \bar{\theta}_j(\zeta) + \frac{Bi_{\eta 1}^*}{Cj_1} \theta_{w1}(\zeta) \\ \frac{d\theta_{w2}'}{d\zeta} &= \frac{1}{Cj_2} \sum_{j=1}^N \frac{1}{N_j} \frac{\partial \psi_j}{\partial \eta} \Big|_{\eta=1} \bar{\theta}_j(\zeta) + \frac{Bi_{\eta 2}^*}{Cj_2} \theta_{w2}(\zeta)\end{aligned}\quad (14a,b)$$

The boundary conditions for the transformed temperatures and wall temperatures are given by:

$$\bar{\theta}_i(\zeta) = \bar{f}_i \quad \zeta = 0, \quad \bar{\theta}_i'(\zeta) = 0 \quad \zeta = l_\zeta, \quad i = 1, 2, \dots, N \quad (14c,d)$$

$$\frac{d\theta_{w1}}{d\zeta} \Big|_{\zeta=0} = 0; \quad \frac{d\theta_{w1}}{d\zeta} \Big|_{\zeta=l_\zeta} = 0; \quad \frac{d\theta_{w2}}{d\zeta} \Big|_{\zeta=0} = 0; \quad \frac{d\theta_{w2}}{d\zeta} \Big|_{\zeta=l_\zeta} = 0 \quad (14e-h)$$

where

$$\bar{f}_i = \int_0^1 W(\eta) \psi_i(\eta) (1 - \theta_p(\eta)) d\eta \quad (14i)$$

Due to the slower convergence rates expected from the above formal solution once the inverse formula is substituted back into Eq. (12c), as noted in [17,18], the energy equation is integrated across the transversal domain, as described in [23,24] and named as the integral balance scheme, in order to reach an improved convergence behavior in the representation of the derivatives and temperatures at the boundary positions. Thus, the fluid energy equation is integrated across the channel, and the inverse formula is substituted for the bulk temperature within the convection term, providing alternative expressions for the boundary derivatives. This procedure can be found in detail in [11].

Thus, the following ODE system truncated to order N is to be solved:

$$\{Y'(\zeta)\} = [C]\{Y(\zeta)\} \quad (15a)$$

$$Y = \left\{ \bar{\theta}_1(\zeta), \bar{\theta}_2(\zeta), \dots, \bar{\theta}_N(\zeta), \bar{\theta}_1'(\zeta), \bar{\theta}_2'(\zeta), \dots, \bar{\theta}_N'(\zeta), \bar{\theta}_{w1}(\zeta), \bar{\theta}_{w2}(\zeta), \bar{\theta}_{w1}'(\zeta), \bar{\theta}_{w2}'(\zeta) \right\}^T \quad (15b)$$

which requires the computation of the eigenvalues and eigenvectors of matrix C to yield the solution vector Y , or:

$$(C - I\lambda)\xi = 0, \quad Y(\zeta) = \sum_{k=1}^{N+4} c_k \xi_k e^{\lambda_k \zeta} \quad (15c,d)$$

It should be noticed that the averaged wall temperatures, $\theta_{w1}(\zeta)$ and $\theta_{w2}(\zeta)$, are directly obtained from the solution vector $Y(\zeta)$ as positions N+1 and N+2, as well as their longitudinal derivatives (positions N+3 and N+4).

The fluid bulk temperature is given by the working expression below:

$$\theta_{av}(\zeta) = \frac{\sum_{i=1}^N \int_0^1 W(\eta) \psi_i(\eta) d\eta \frac{\bar{\theta}_i(\zeta)}{N_i}}{\int_0^1 W(\eta) d\eta} + \frac{\int_0^1 W(\eta) \theta_p(\eta) d\eta}{\int_0^1 W(\eta) d\eta} \quad (16)$$

For the computation of the associated local Nusselt numbers, the derivatives at the walls of the fluid temperature are obtained by making use of the expressions previously derived with the integral balance scheme, or simply in the more direct form illustrated below for wall 1:

$$Nu_1 = \frac{-2 \left(\sum_{i=1}^{\infty} \frac{d\psi_i(\eta)}{d\eta} \Big|_{\eta=0} \frac{\bar{\theta}_i(\zeta)}{N_i} + \frac{d\theta_p(\eta)}{d\eta} \Big|_{\eta=0} \right)}{\theta_{w1}(\zeta) - \theta_{av}(\zeta)} \quad (17)$$

3. Experimental Analysis

Before obtaining the experimental results for the proposed covalidation effort, two prior steps were required, namely, the design and fabrication of the microchannels, and the assembly of an experimental platform that would allow for the easy exchange of different microchannel setups. A PMMA (*poly-methyl methacrylate*) prism of low thermal conductivity was employed as the structural support of the metallic plates that form the microchannels, chosen to be made of electronic grade copper (upper plate) and brass (lower plate). Micro-machining of the PMMA block and of the metallic plates was accomplished and the setup was assembled according to Figures 2 below.

Figures 3 show the assembled microchannel setup, within the PMMA block, and the installed thermocouples at both the lower (Fig.3.a) and the upper (Fig.3.b) plates. The employed technique allowed for the fabrication of microchannels up to 20 μ m of plates spacing and uncertainty of $\pm 2.0\mu$ m.

The complete experimental platform is shown in Figure 4 below, which is fully automated, both in the data acquisition and on the control of the flow and heating parameters. The concept was that of allowing for straightforward interchanges of the microchannel setups without modifications of the remaining of the platform.

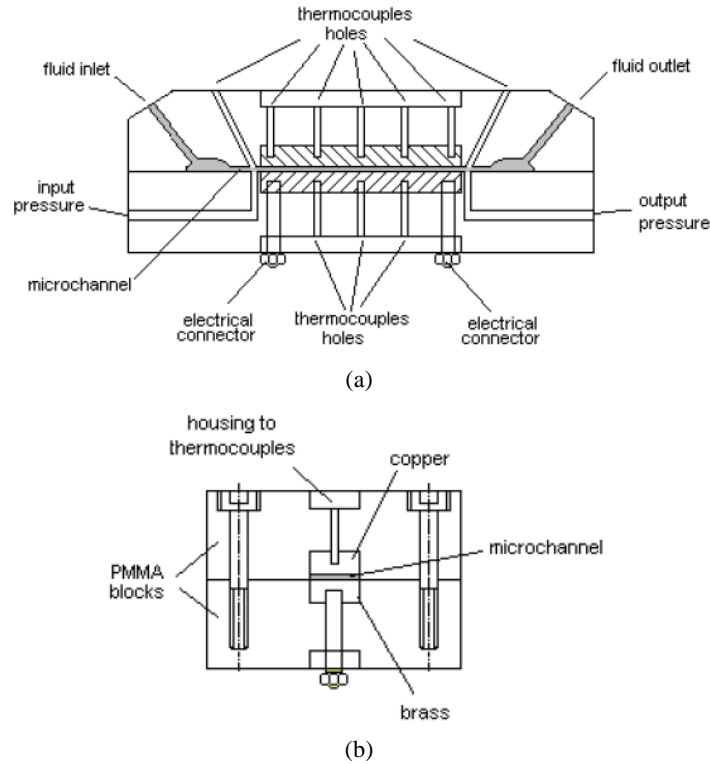


Figure 2. a) Schematic representation of the microchannel assembly; b) Cross section view of the assembly.

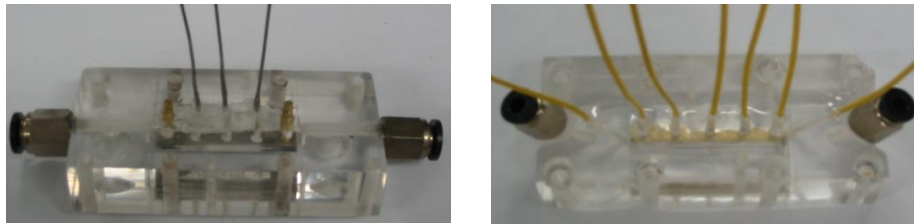


Figure 3. Details of the lower and upper plates of the microchannel setup with installed thermocouples.

The microchannel wall was heated by Joule effect through an alternate current circuit of 220 V and 33 A. Temperature measurements were taken with type E (chromel-constantan) and type K (chromel-alumel) thermocouples, with uncertainty to within 0.3°C. Pressure difference measurements were obtained with membrane type pressure transducers, model S10 from WIKA Alexander Wiegand GmbH & C.KG, 0-10 bar (4 to 20 mA). Mass flow rate was determined with the aid of an electronic scale MARTE model AS 2200 (0-2000g, ± 0.0001g).



Figure 4. General view of the experimental platform.

Figure 5 below shows a schematic representation of the experimental apparatus, where each one of the constructive elements is identified. The acquisition system was based on a Pentium IV microcomputer with 2Gb of RAM, HD of 80Mb, and RS 232 and USB connections, also functioning as a “data logger”. The system employed was the Compact Field Point of National Instruments, model CFP 2000, with one module for acquisition of temperature through resistance, two modules for temperature acquisition through thermocouples, and one module for acquisition with current, as can be observed in Figures 6. The software LabView 8.0 was utilized in the construction of the control and acquisition computer code, including the statistical data treatment and the uncertainty analysis of the incorporated measurements.

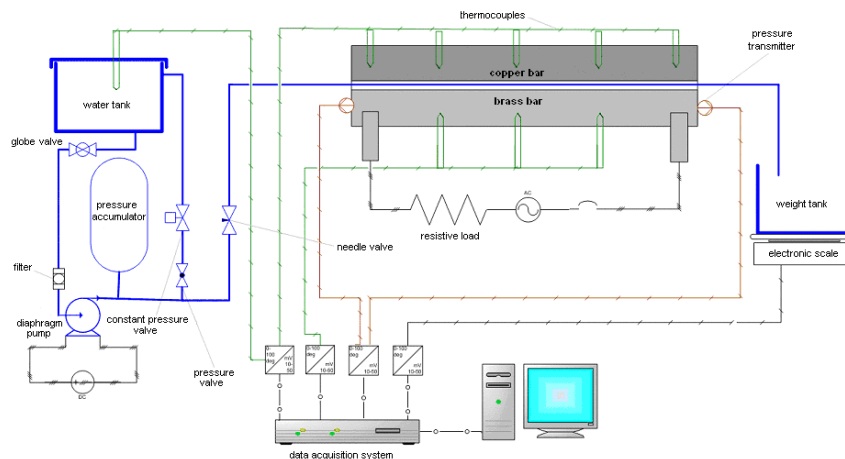


Figure 5. Schematic representation of the experimental apparatus.



Figure 6. a) CFP2000 acquisition system with the acquisition and signal processing modules, b) screen of the code constructed with LabView 8.0 for control and acquisition.

An additional computational code was developed on the *Mathematica* 7.0 system for determining the propagation of uncertainties up to the evaluation of the local Nusselt numbers, based on the measurements of temperature, mass flow rate, channel dimensions, and the power generated by Joule effect in the copper bar at the bottom of the channel, through the resistance and potential difference measurements on the bar. Table 1 below shows uncertainties associated to the each experimental measurement, used to calculate the uncertainty of the experimental Nusselt numbers. The uncertainty estimated for the local Nusselt number experimental results was around 11.6%.

4. Results and Discussion

The first step in the present implementation of the conjugated heat transfer problem in microchannels was to compare and validate the obtained results with published ones for the symmetric case [16,19], also obtained through GITT but not accounting for heat generation within the walls and within the fluid by viscous dissipation, and for axial heat conduction along the fluid. In

both sets of results the observed agreement was quite good, and the present implementation reproduces slightly more closely the more recent implementation in [19]. It should be noted that truncation orders of up to $N=30$ were employed in the present simulation.

TABLE 1. Uncertainties associated to each individual measurement that compose the uncertainty of the Nusselt number.

Parameter	Uncertainties	Meter	Reading
Time	0,01%	clock / CPU	LW
Mass	2,0%	Scale	R-232 / LW
Pressure	1,0%	Transmitter pressure	cFP-22/LW
Temperature	0,3%	PT-100	cFP-22/LW
Temperature	0,8%	Thermocouple E	cFP-22/LW
Temperature	0,8%	Thermocouple K	cFP-22/LW
Dimensions	0,3 μm	Digital micrometer	manual
Voltage	1,5%	Digital multimeter	manual
Current	1,5%	Digital multimeter	manual

Next, the proposed asymmetric model was verified through experimental measurements on the parallel plates micro-channel micro-machined from metallic plates of copper and brass, with adjustable spacing. The lower plate is heated by Joule effect and the whole set was encapsulated in the acrylic casing, being cooled by distilled water. Temperature measurements were then taken within both plates, and compared with the simulation results for the lumped wall temperatures along the channel length. The range of Reynolds number analyzed was approximately from $Re=10$ to 250. Sample graphs of such comparisons are shown in Figure 7 below, for a parallel plates spacing of 270 microns, and $Re=13$, 64, 122, and 224, and in Figure 8 for $Re=15$, 47, 64 and 151. The two sets of curves were taken in different runs, so as to also provide a repeatability analysis. The curves to the left refer to the measurements at the heated bottom wall, while the curves to the right are temperatures measured at the top wall. The agreement between theoretical and experimental wall temperature values is indeed quite reasonable, except at the last set of curves in each figure, related to the very low values of Reynolds number. One may also observe the marked influence of the Reynolds number on the heat transfer behavior throughout this range, with the noticeable loss of adherence of the theoretical results for lower values of Re ($Re=13$ in Fig.7 and $Re=15$ in Fig.8). Also, the model here proposed does not account for heat losses at the walls ends and for axial heat flow towards the entry tubing of the channel, beyond the heat

transfer section, which start playing some role for such lower values of Peclet number, and thus reducing the temperature gradients along the walls.

Figure 9 provides the theoretical predictions of the dimensionless walls temperature distributions along the channel length, for the same values of Reynolds numbers as considered in Figure 7. Clearly, the present model predicts that the temperature differences between the entrance and exit are less marked for the higher values of Re, while more significant temperature variations along the channel are observable at the lower values of Re, towards the channel exit. In fact, the proposed formulation does not account for heat losses at the fluid and walls ends, which are seen to be significant at low Re.

Table 2 brings a comparison of theoretical and experimental local Nusselt numbers at the middle of the channel length ($x=L/2$) and at the end ($x=L$), together with the corresponding values of Reynolds and Prandtl numbers, and conjugation parameters at the bottom and top walls. It can be seen that the conjugation parameters grow from around 10^{-4} for the higher values of Re, to almost 1 at the lower value of Re around 10. The model seems to account reasonably well for the physical effects, predicting the Nusselt numbers at both axial positions to within a maximum deviation of 3% in the range of parameters here investigated, with a slightly higher deviation for decreasing Reynolds number.

TABLE 2. Comparison of simulation and experiments for local Nusselt numbers in microchannel ($x=L/2$ and $x=L$).

Re	Pr	Cj1	Cj2	Nu _{th} (L/2)	Nu _{exp} (L/2)	Nu _{th} (L)	Nu _{exp} (L)
242.2	6.48	2.86×10^{-4}	1.17×10^{-3}	5.072	5.068	4.683	4.715
206.1	6.27	4.26×10^{-4}	1.74×10^{-3}	4.926	4.987	4.628	4.672
151.2	6.25	7.86×10^{-4}	3.21×10^{-3}	4.755	4.823	4.581	4.587
122.2	6.33	1.18×10^{-3}	4.80×10^{-3}	4.675	4.738	4.566	4.545
102.4	5.94	1.89×10^{-3}	7.71×10^{-3}	4.615	4.656	4.561	4.503
79.47	5.76	0.00332	0.0136	4.576	4.580	4.556	4.466
65.34	6.18	0.00429	0.0175	4.569	4.553	4.555	4.453
47.45	5.33	0.00947	0.0386	4.554	4.485	4.547	4.485
15.44	5.52	0.0954	0.389	4.509	4.380	4.488	4.499
10.82	5.01	0.234	0.955	4.473	4.385	4.440	4.374

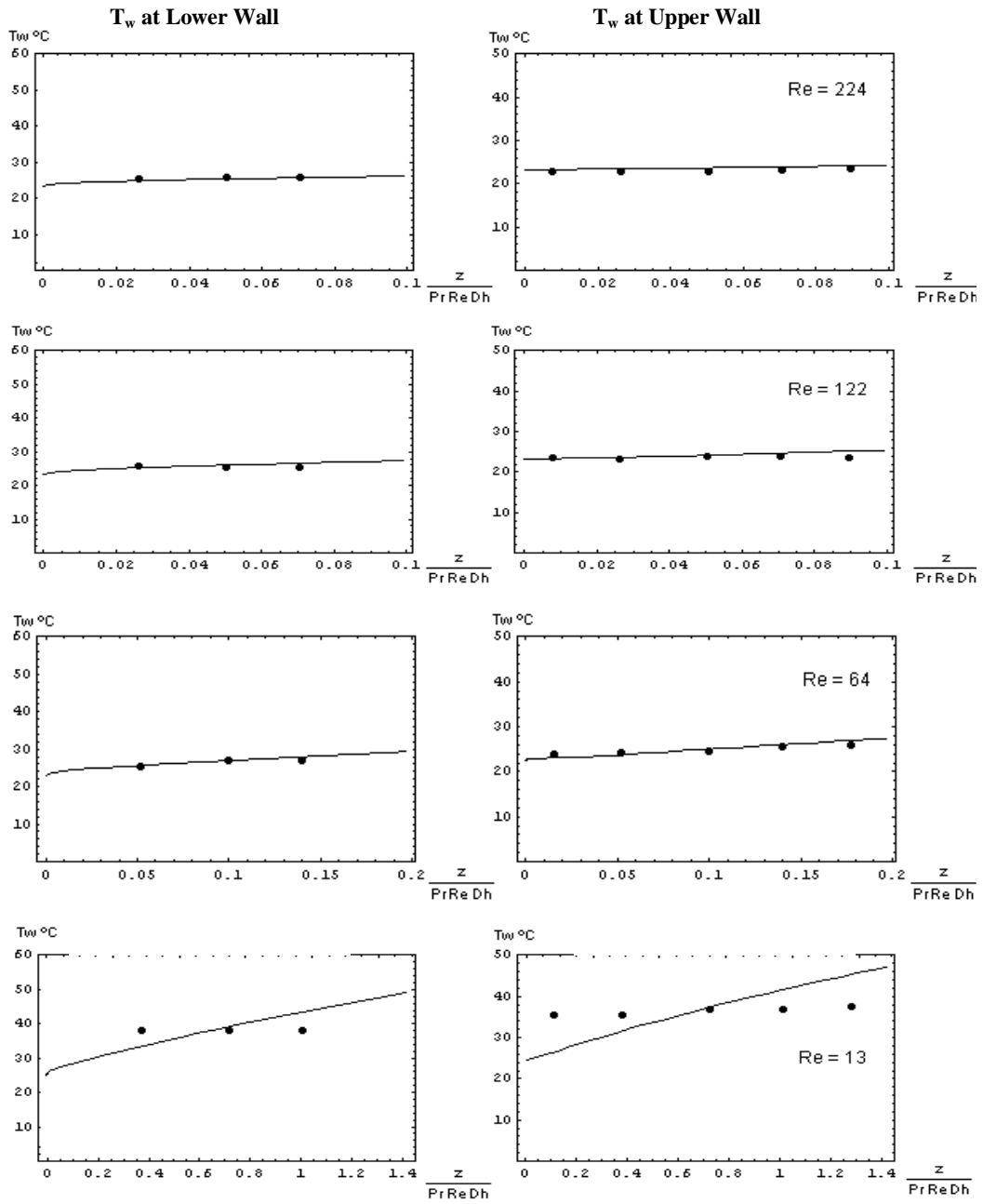


Figure 7. Comparison of measured (dots) and calculated (solid lines) wall temperatures for $Re=224, 122, 64$ and 13 . (bottom heated plate– left, top unheated plate – right).

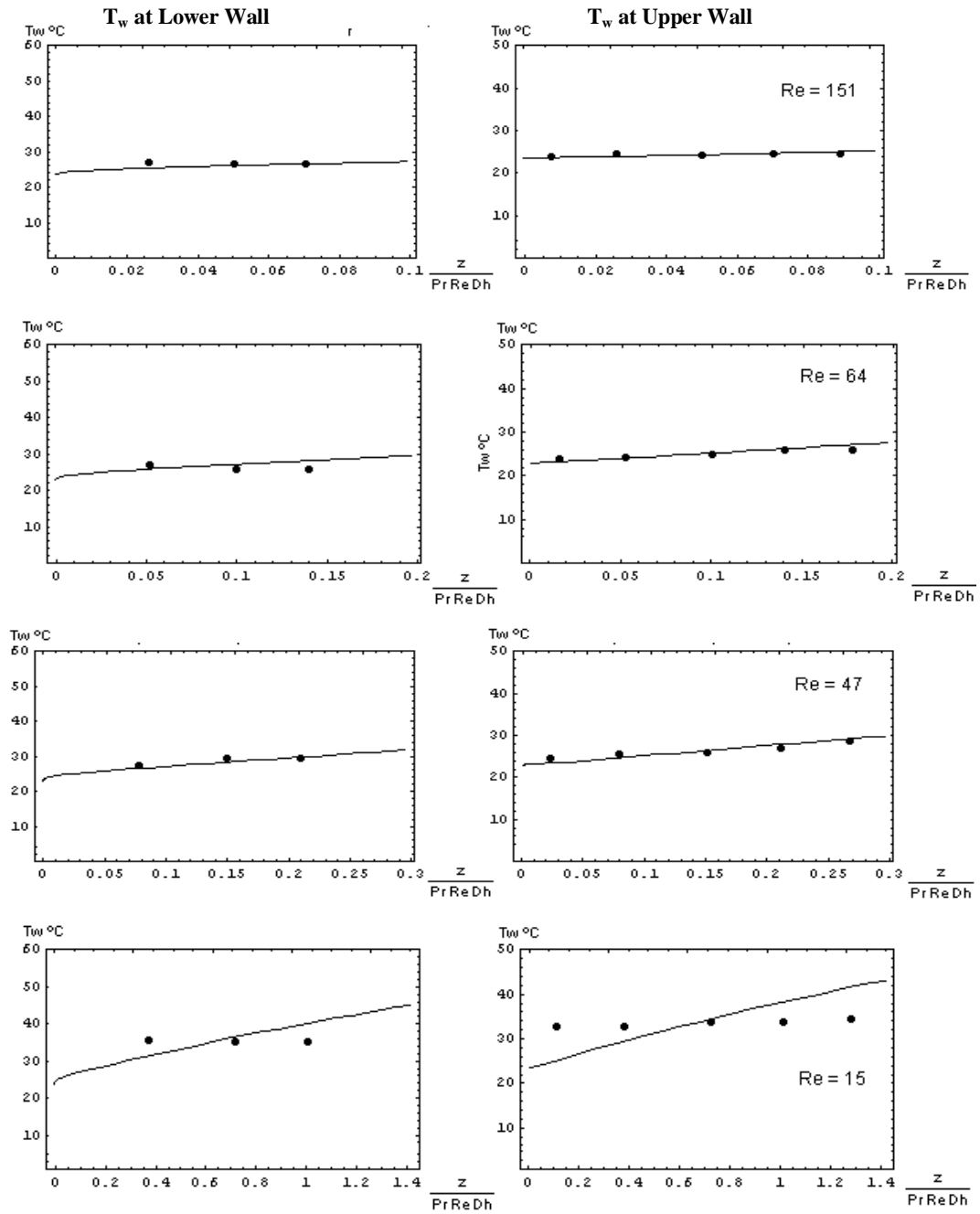


Figure 8. Comparison of measured (dots) and calculated (solid lines) wall temperatures for $Re=151, 64, 47,$ and $15.$ (bottom heated plate– left, top unheated plate – right).

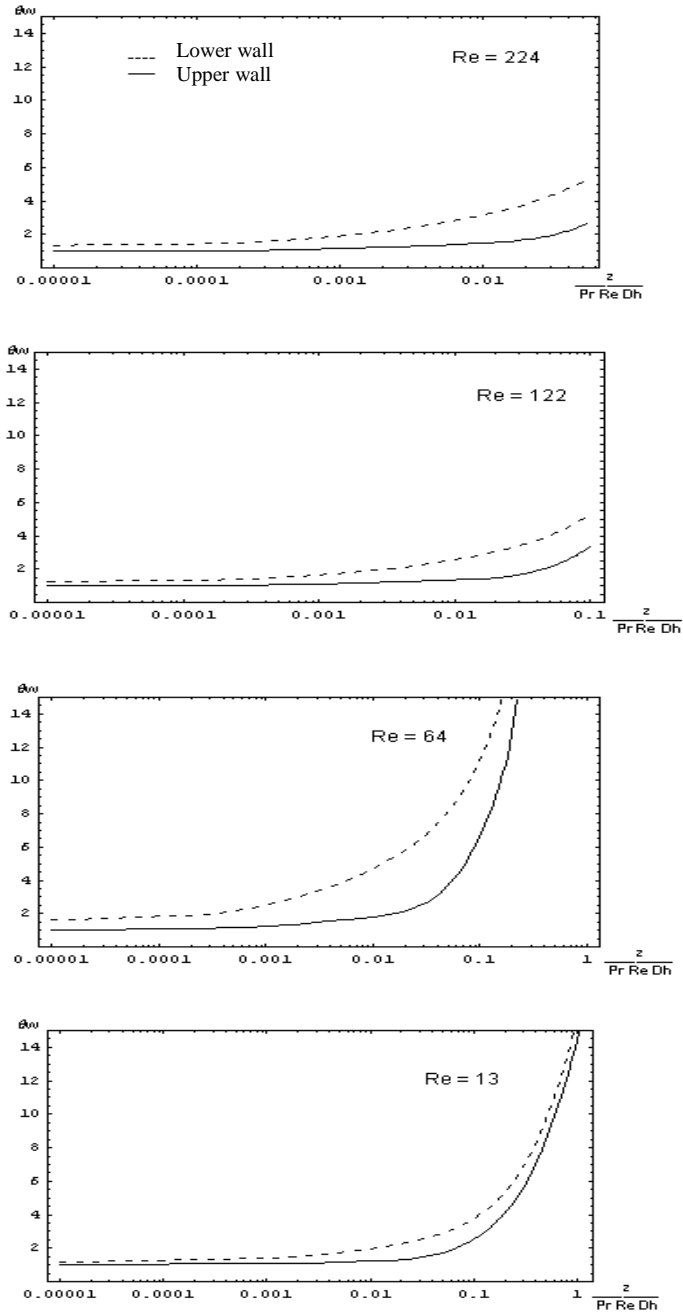


Figure 9. Theoretical prediction of the dimensionless walls temperature distributions along the channel length for different Reynolds numbers, Re=224, 122, 64 and 13. (bottom plate–dashed, top plate – solid line).

The experimental results for the local Nusselt numbers may also be examined over Figure 10 below, where the results are encapsulated by the theoretical values of the limiting situations of prescribed wall temperatures and prescribed wall heat fluxes. It can be noticed that for lower values of Re , when the conjugation parameters also markedly grow (see Table 2), the obtained Nusselt numbers approach the limiting solution of a prescribed uniform wall temperature, due to the longitudinal wall heat conduction effect. As the Reynolds number increases, the Nusselt number starts migrating towards the prescribed wall heat flux condition, with the progressive reduction of the conjugation effects. It should also be observed that for the higher values of Re , the Nusselt number values at $x=L/2$ and $x=L$ deviate significantly, since at the middle of the channel (and eventually even at the end) one has not yet reached a fully developed condition, such as for the lower values of Re where they practically coincide.

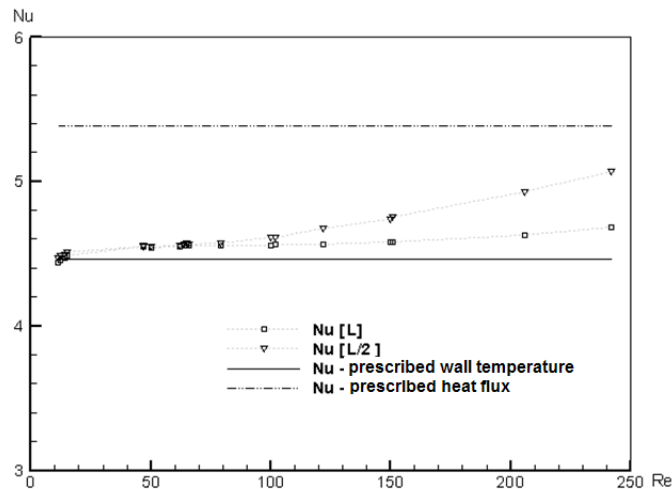


Figure 10. Comparison of measured (dots) local Nusselt numbers for parallel-plates microchannel against limiting fully developed values for prescribed wall temperature (solid line) and heat flux (dashed line) (Reynolds number ranging from 10 to 242).

In conclusion, the influence of conjugated convection-conduction heat transfer in microchannels was investigated, considering an asymmetric parallel-plates configuration, with heat generation within the walls, besides axial heat diffusion and viscous dissipation in the fluid. An experimental setup was built to measure the wall temperatures and evaluate Nusselt numbers along a brass-copper microchannel with 270 microns spacing between the parallel plates, heated at the bottom brass plate. In the range of parameters analyzed ($10 < Re < 250$), the relevance of wall conjugation was verified, and the simulated results provided an agreement within 3% against the experimental local Nusselt numbers along the channel. Conjugation

deviates the thermal boundary condition from the expected simplified model of applied uniform heat flux, and at limiting situations brings the system behavior even closer to that of a prescribed uniform temperature case. Thus, the simplified uniform wall heat flux modeling can induce an erroneous interpretation of heat transfer augmentation once conjugation effects are not accounted for in the interpretation of experimental results, which might aid in partially explaining discrepancies observed among experimental results in microchannels and classical correlations for internal forced convection built for macroscale situations [3, 13].

ACKNOWLEDGEMENTS

The authors would like to acknowledge the financial support provided by CNPq and CAPES, sponsoring agencies in Brasil.

REFERENCES

1. C.B. Sobhan and G.P. Peterson, *Microscale and Nanoscale Heat Transfer: Fundamentals and Engineering Applications*, CRC Press, Boca Raton, FL (2008).
2. Y. Yener, S. Kakaç, M. Avelino, and T. Okutucu, Single-phase Forced Convection in Micro-channels – a State-of-the-art Review, in: S. Kakaç, L.L. Vasiliev, Y. Bayazitoglu, Y. Yener. (Eds.), *Microscale Heat Transfer – Fundamentals and Applications*, NATO ASI Series, Kluwer Academic Publishers, Netherlands, pp.1-24 (2005).
3. G.L. Morini, Single-Phase Convective Heat Transfer in Microchannels: a Review of Experimental Results, *Int. J. of Thermal Sciences*, 43, 631-651 (2004).
4. M.D. Mikhailov and R.M. Cotta, Mixed Symbolic-Numerical Computation of Convective Heat Transfer with Slip Flow in Microchannels, *Int. Comm. Heat & Mass Transfer*, 32, 341-348 (2005).
5. R.M. Cotta, S. Kakaç, M.D. Mikhailov, F.V. Castellões, C.R. Cardoso, Transient Flow and Thermal Analysis in Microfluidics, in: S. Kakaç, L.L. Vasiliev, Y. Bayazitoglu, Y. Yener. (Eds.), *Microscale Heat Transfer – Fundamentals and Applications*, NATO ASI Series, Kulwer Academic Publishers, Netherlands, pp. 175-196 (2005).
6. S. Yu and T.A. Ameel, Slip Flow Heat Transfer in Rectangular Microchannels, *Int. J. Heat Mass Transfer*, 44, 4225-4234 (2001).
7. G. Tunc and Y. Bayazitoglu, Heat Transfer in Microtubes with Viscous Dissipation, *Int. J. Heat Mass Transfer*, 44, 2395-2403 (2001).

8. G. Tunc and Y. Bayazitoglu, Heat Transfer in Rectangular Microchannels, *Int. J. Heat Mass Transfer*, 45, 765-773 (2002).
9. F.V. Castellões and R.M. Cotta, Analysis of Transient and Periodic Convection in Micro-channels via Integral Transforms, *Progress in Computational Fluid Dynamics*, 6, 321-326 (2006).
10. F.V. Castellões, C.R. Cardoso, P. Couto, and R.M. Cotta, Transient Analysis of Slip Flow and Heat Transfer in Microchannels, *Heat Transfer Engineering*, 28, 549-558 (2007).
11. J.S. Nunes, P. Couto, and R.M. Cotta, Conjugated Heat Transfer Problem in Rectangular Micro-channels under Asymmetric Conditions, Proc. of 5th National Congress of Mechanical Engineering, CONEM 2008, ABCM, Paper no. CON08-0739, Salvador, BA, August 2008.
12. F.V. Castellões and R.M. Cotta, Heat Transfer Enhancement in Smooth and Corrugated Microchannels, Proc. of the 7th Minsk Int. Seminar on Heat Pipes, Heat Pumps, Refrigerators, Invited Lecture, Minsk, Belarus, 8-11 September 2008.
13. G. Maranzana, I. Perry, and D. Mailliet, Mini- and Micro-channels: Influence of Axial Conduction in the Walls, *Int. J. Heat and Mass Transfer*, 47, 3993-4004 (2004).
14. Y.L. Perelman, On Conjugate Problems of Heat Transfer, *Int. J. Heat and Mass Transfer*, 3, 293-303 (1961).
15. A.V. Luikov, V.A. Aleksashenko, and A.A. Aleksashenko, Analytical Methods of Solution of Conjugated Problems in Convective Heat Transfer, *Int. J. Heat and Mass Transfer*, 14, 1047-1056 (1971).
16. R.O.C. Guedes, R.M. Cotta, and N.C.L. Brum, Conjugated Heat Transfer in Laminar Flow Between Parallel - Plates Channel, 10th Brazilian Congress of Mechanical Engineering, Rio de Janeiro, Brazil, 1989.
17. R.O.C. Guedes, R.M. Cotta, and N.C.L. Brum, Heat Transfer in Laminar Tube Flow with Wall Axial Conduction Effects, *J. Thermophysics & Heat Transfer*, 5 (4), 508-513 (1991).
18. R.O.C. Guedes and R.M. Cotta, Periodic Laminar Forced Convection within Ducts Including Wall Heat Conduction Effects, *Int. J. Eng. Science*, 29 (5), 535-547 (1991).
19. F.G. Elmor, R.O.C. Guedes, and F.N. Scofano, Improved Lumped Solution for Conjugate Heat Transfer In Channel Flow with Convective Boundary Condition, *Int. J. Heat & Technology*, pp.78-88 (2005).
20. C.P. Naveira, M. Lachi, R. M. Cotta, and J. Padet, Hybrid Formulation and Solution for Transient Conjugated Conduction-External Convection, *Int. J. Heat & Mass Transfer*, 52, 112-123 (2009).
21. C.P. Naveira-Cotta, M. Lachi, M. Rebay, and R.M. Cotta, "Comparison of Experiments and Hybrid Simulations of Transient Conjugated Conduction-Convection-Radiation, ICCHMT International Symposium on Convective Heat and Mass Transfer in Sustainable Energy, CONV-09, Yasmine Hammamet, Tunisia, April 2009.
22. S. Wolfram, S., The *Mathematica* Book, version 7.0, Cambridge-Wolfram Media (2008).
23. R.M. Cotta, Integral Transforms in Computational Heat and Fluid Flow, CRC Press, USA (1993).

24. R.M. Cotta and M.D. Mikhailov, *Heat Conduction: Lumped Analysis, Integral Transforms, Symbolic Computation*, Wiley-Interscience, NY (1997).
25. R.M. Cotta, *The Integral Transform Method in Thermal and Fluids Sciences and Engineering*, Begell House, New York (1998).
26. R.M. Cotta and M.D. Mikhailov, *Hybrid Methods and Symbolic Computations*, in: W.J. Minkowycz, E.M. Sparrow, and J.Y. Murthy (Eds.), *Handbook of Numerical Heat Transfer*, 2nd ed., Wiley, NY, pp. 493-522 (2006).